*Oxidation of Metals, Vol. 41, Nos. 1/2, 1994*

# Sulfidation–Oxidation Behavior of Alloy 800H in $SO_2-O_2$ and $H_2-H_2S-CO-CO_2$ Atmospheres

**H. Xu,* M. G. Hocking,* and P. S. Sidky***

*Received October 22, 1992; revised September 15, 1993*

*The high-temperature-corrosion behavior of alloy 800H has been studied in an oxidizing ($SO_2-O_2$, $P_{O_2} = 0.23$ atm, $P_{S_2} = 1.9 \times 10^{-29}$ atm) and a reducing ($H_2-H_2S-CO-CO_2-N_2$, $P_{O_2} = 1.5 \times 10^{-18}$ atm $P_{S_2} = 4.3 \times 10^{-8}$ atm, $a_c = 0.03$) sulfidizing environment, at 750°C and 850°C, respectively. When corroded in $SO_2-O_2$, the protective chromia scale which developed on the alloy in the early stages cracked and spalled in quite a short time period. This led to the growth of iron and nickel sulfides beneath the chromia layer, causing more chromia spallation. When corroded in $H_2-H_2S-CO-CO_2-N_2$, the alloy exhibited breakaway corrosion in about 35 hr, at which stage liquid nodules formed on the sample surface. The nodules were studied in detail and were found to consist of three layers. The growth mechanism of such nodules is proposed.*

**KEY WORDS:** sulfidation; oxidation; alloy 800H, $SO_2-O_2$; $H_2-H_2S$.

## INTRODUCTION

Industrial, gaseous, sulfidizing environments at elevated temperatures can be broadly divided into two categories: an oxidizing one with sulfur mainly in the form of $SO_2$, and a reducing one with sulfur mainly as $H_2S$. The former is typical of gas turbine and waste incineration environments, with a high $P_{O_2}$ and low $P_{S_2}$. The latter is found in coal-gasification atmospheres (CGA), and usually has a high $P_{S_2}$ ($>10^{-10}$ atm) and a low $P_{O_2}$ ($<10^{-15}$ atm).

*Department of Materials, Imperial College, London SW7 2BP, UK.



0030-770X/94/1200-0081$07.00/0 

Laboratory studies of high-temperature corrosion in $SO_2 - O_2$ or $SO_2$ have been going on for the last 30 years. Pure metals (e.g., Ni) and simple systems (e.g., binary and some ternary alloys) are most often used for mechanistic studies. In $SO_2 + O_2$ atmospheres, the thermodynamic stable phases for Ni, Fe, and Co are very often their sulfates, and it has been established that a thin layer of sulfate is responsible for the high corrosion rates of metals and alloys.[1-3] A network of sulfides within the scale provides a rapid diffusion path for cations.[4]

High-temperature corrosion in reducing atmospheres ($H_2-H_2S$, $H_2-H_2O-H_2S$, $H_2-H_2S-CO-CO_2$, etc.) has received much interest since the late 1970s. Thermodynamic-stability diagrams are an indispensible tool in such studies. Except for $Cr_2O_3$, the stable phases for Ni, Fe, and Co are usually their sulfides in this type of atmosphere. Investigations on the initial stage of corrosion of metals and alloys confirmed the simultaneous nucleation of both $Cr_2O_3$ and CrS as well as other sulfides.[5-6] Natesan and co-workers[7-8] found after extensive work that the $P_{O_2}$ required for the formation of a continuous $Cr_2O_3$ layer on an alloy is at least $10^3$ times higher than the thermodynamic value defined by $Cr-Cr_2O_3$ equilibrium, and this threshold value was termed the kinetics boundary. However, outward cation diffusion through the $Cr_2O_3$ layer also plays an important part in the later stages of corrosion and may lead to breakaway corrosion eventually. Therefore, logically, the kinetics boundary of a particular alloy in a certain atmosphere is a function of the alloy's exposure time in the atmosphere. If a continuous $Cr_2O_3$ layer is expected after a longer period of time, a higher $P_{O_2}$ is needed.

Several Ni-, Fe-, and Co-base superalloys have recently been studied in both kinds of sulfidizing atmospheres in this laboratory. The corrosion mechanism of a Ni–Co–Cr–Si superalloy in an $SO_2 - O_2$ (2:1) atmosphere has been reported.[3] This paper reports on the high-temperature-corrosion behavior of alloy 800H in an $SO_2 - O_2$ and a $H_2-H_2S-CO-CO_2-N_2$ environment with the emphasis on the latter.

## EXPERIMENTAL PROCEDURES

The alloy is supplied by Haynes International Ltd. and has the following nominal composition:

| Ni | Co | Fe | Cr | C | Mn | Si | Al | Ti |
|---|---|---|---|---|---|---|---|---|
| 33 | 2 maximum | Bal | 21 | 0.07 | 1.5 | 1.0 | 0.4 | 0.4 |

Alloy samples were approximately 8 × 8 × 2 mm in size and polished on SiC papers from 400 till 800 sequentially. Each sample was ultrasonically cleaned in acetone prior to an experiment. Samples for $SO_2 - O_2$ corrosion tests were slightly polished on their corners to avoid severe preferential attack on the sharp edges.

## $SO_2 - O_2$

The corrosion tests in $SO_2 - O_2$ gases were carried out at 750°C. The gases of $SO_2$ and $O_2$ were premixed in a gas train at 66 ml/min and 33 ml/min, respectively, giving an $SO_2$:$O_2$ ratio of 2:1 at room temperature. The total pressure inside the furnace was maintained at 1 atm. This gives $P_{O_2} = 0.23$ atm, $P_{S_2} = 1.9 \times 10^{-29}$ atm at 750°C.

The apparatus has been described elsewhere.[9] A sample was hung on a silica hook below a Pt crucible which acted as a catalyst. The system was flushed with the corrosion gases for 30 min before the furnace was lifted up to locate the specimen in the hot zone.

## $H_2$–$H_2S$–CO–$CO_2$–$N_2$

Tests in the $H_2$–$H_2S$–CO–$CO_2$–$N_2$ gas mixture with the following composition at room temperature were made at 850°C:

| Gas | $H_2$ | $H_2S$ | CO | $CO_2$ | $N_2$ |
|---|---|---|---|---|---|
| Volume% | 17.6 | 0.106 | 20.8 | 20.1 | Balance |

This gives $P_{O_2} = 1.5 \times 10^{-18}$ atm, $P_{S_2} = 4.3 \times 10^{-8}$ atm and $a_c = 0.03$ at 850°C.

The gas mixture went into the furnace reaction tube from the bottom and was sucked out by a water pump through a side arm at the top. A baffle system was designed.[10] This maintained the total pressure inside the reaction tube at 1 atm while preventing any lab air from going into the tube, and allowed continuous monitoring of the weight change of the sample.

A sample was hung on a silica hook. The system was flushed with the gas mixture for 30 min before the furnace was quickly lifted up to locate the specimen in the hot zone.

After corrosion, X-ray diffraction phase analysis (XRD) was carried out to identify corrosion products. A scanning electron microscope (SEM) with an energy-dispersive X-ray spectrometer (EDS) was employed for both morphologies and chemical analysis. Optical microscopy was applied where appropriate.

## RESULTS AND DISCUSSION

### In $SO_2 - O_2$

The kinetics curve for this alloy at 750°C is shown in Fig. 1. Its nonsmooth characteristics are an indication of the cracking and rehealing of the oxide scales during corrosion. The initial $Cr_2O_2$ spalled off after approximately 62 hr. Two duplicate tests were made and spallation occurred between 25 and 40 hr.

The identified phases with XRD on the surface of the samples after corrosion were $Cr_2O_3$, $FeCr_2O_4$, $Fe_3O_4$, FeS, $Ni_3S_2$, and possibly $(Ni, Fe)SO_4 \cdot H_2O$. One is reminded here that these were the samples after the spallation of scales. Figure 2 shows the SEM surface morphologies of the samples. With the help of XRD results and EDS mapping of the surface, it was found that the subscales are $Cr_2O_3$ as well, probably as a healing layer (Fig. 2a). Some small residues of the initial outer scale of $Cr_2O_3$ can still be seen (Fig. 2b). EDS analysis showed that the bubble like products on the outer scale are iron and nickel sulfides. Cracks can be seen on the subscales as shown in Figs. 2c, 2d. FeS and $Ni_3S_2$ formed underneath the subscales and are most likely to be responsible for the cracking. There seems to be no evidence that the $Ni-Ni_3S_2$ eutectic has formed.

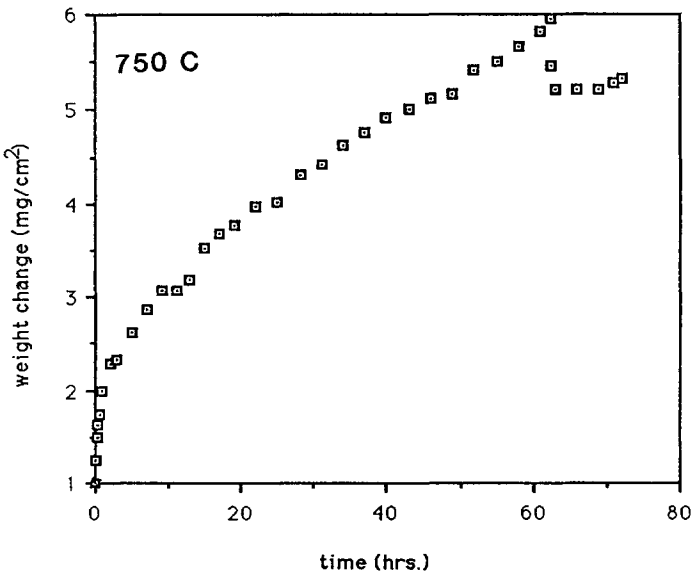


**Fig. 1.** Kinetics curve of alloy 800H in the $SO_2-O_2$ atmosphere.

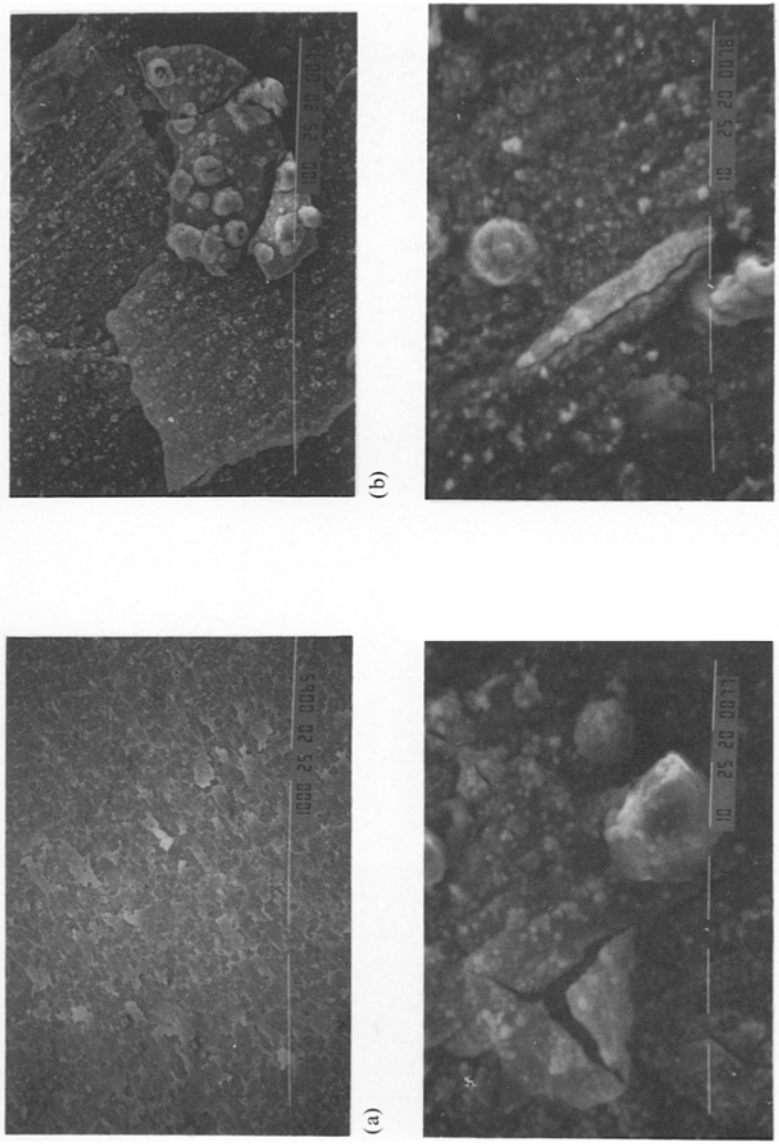

**Fig. 2.** SEM micrographs of alloy 800H after 72 hr of corrosion in $SO_2-O_2$ (2:1) at 750°C. (a) subscales of mainly $Cr_2O_3$; (b) a piece of residual $Cr_2O_3$ outer scale; (c), (d) microfissures in the subscales.

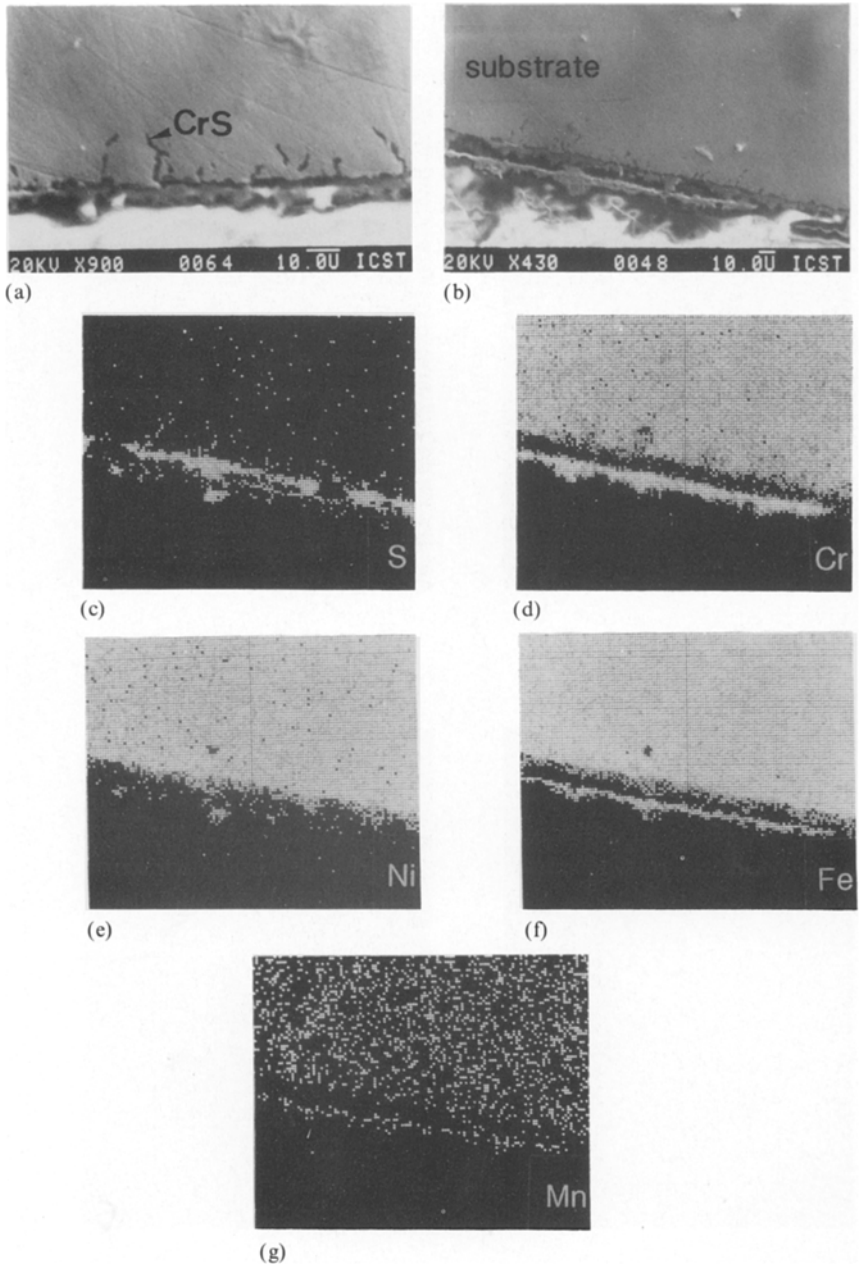


**Fig. 3.** Cross-sectional view of alloy 800H corroded in the $SO_2 - O_2$ (a), (b) SEM pictures; (c)–(g) X-ray maps of (b).

A better understanding of the distribution of corrosion products comes from the X-ray maps of elements on the cross section of the sample with subscales (Fig. 3). Sulfides (FeS and $Ni_3S_2$) formed underneath the $Cr_2O_3$ subscale, and nodules of these can also be found above the subscale. CrS stringers can be found in the alloy substrate along grain boundaries.

It has been proposed that the initial stage of corrosion in this atmosphere is the simultaneous nucleation of FeO, NiO, and $Cr_2O_3$.[3] A continuous $Cr_2O_3$ scale would then undercut the oxides and be formed.

The stable phases can be decided from Fig. 4, and these are $Cr_2O_3$ and Fe, Ni sulfates. (The two thermodynamic-stability diagrams in the paper are both simple superimposition of diagrams for the pure metals of Cr, Fe, Co, and Ni. Phases containing more than one metallic element are not included.). The $FeCr_2O_4$ spinel forms through the following solid-state reaction:

$$FeO + Cr_2O_3 = FeCr_2O_4 \tag{1}$$

There are two kinds of iron sulfates: $FeSO_4$ and $Fe_2(SO_4)_3$. From a more detailed thermodynamic-stability diagram, it was decided that $Fe_2(SO_4)_3$ is the stable one in this case.[11]

The Ni and Fe sulfates form on the top surface of NiO and FeO and give rise to the following reactions, which are rapid corrosion processes:

$$9Ni + 2NiSO_4 = 8NiO + Ni_3S_2 \tag{2}$$

$$10Fe + Fe_2(SO_4)_3 = 3Fe_3O_4 + 3FeS \tag{3}$$

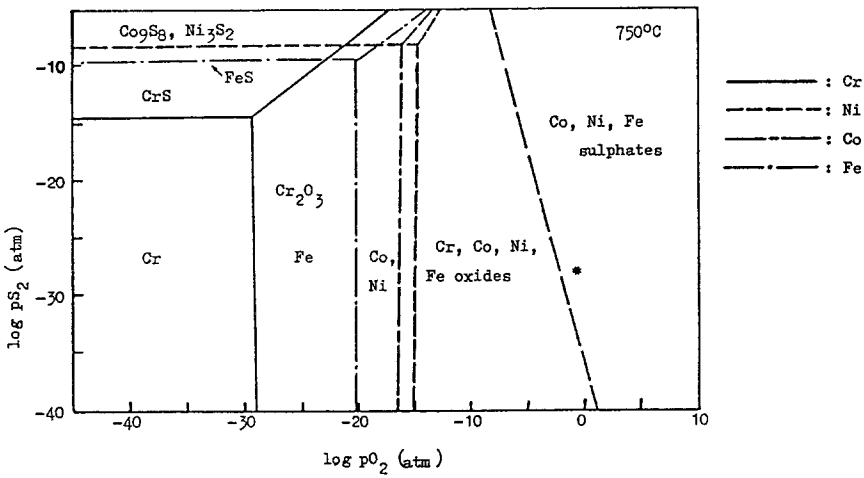


**Fig. 4.** Thermodynamic phase-stability diagrams for the pure metals Cr, Fe, Co, and Ni at 750°C. The asterisk is the equilibrium point of the $SO_2-O_2$ (2:1) atmosphere used in this work.

The presence of sulfates has been previously confirmed by XPS in this work.[3]

Fast-moving species such as Fe and Mn ions diffuse outward through the scales. The ionic radii of both $Fe^{2+}$ and $Mn^{2+}$ (0.87 and 0.91 Å respectively) are larger than that of $Cr^{3+}$ (0.64 Å).[12] The very high Fe

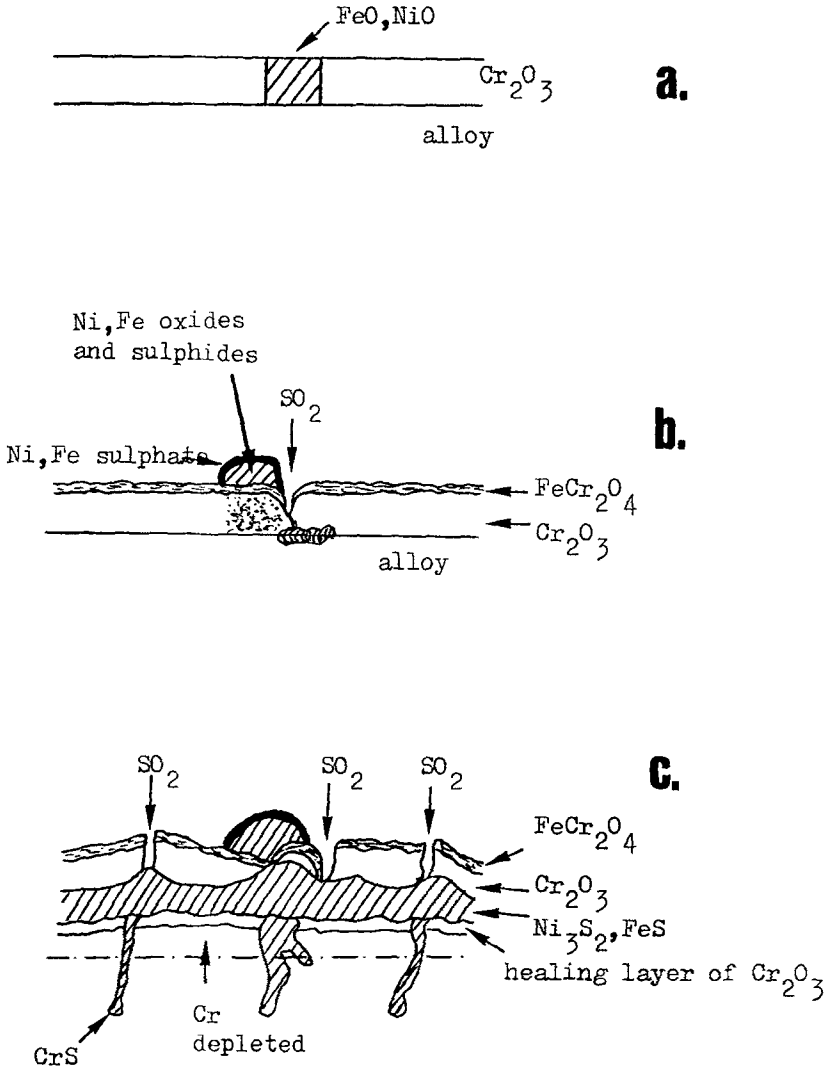


**Fig. 5.** A schematic diagram for the corrosion of alloy 800H in $SO_2$–$O_2$ (2:1) at 750°C before the spalling of $Cr_2O_3$ outer scales. (a) Nucleation of oxides at the initial stage. (b) $SO_2$ penetrates $Cr_2O_3$ through cracks. (c) Sulfides form beneath $Cr_2O_3$.

content (>41%) in the alloy would lead to increased stresses and hence cracks in the $Cr_2O_3$ scale. There is general agreement that scales formed on Fe–Cr alloys are susceptible to cracking.[13]

Although it is difficult to speculate exactly how the $Cr_2O_3$ outer scale failed due to the absence of such scales in the corrosion product, it is reasonable to assume that the cracks in the $Cr_2O_3$ result in direct contact between the gas and the substrate, which lead to the formation of Ni, Fe sulfides beneath the $Cr_2O_3$ scales.

The growth of sulfides underneath the $Cr_2O_3$ led to more cracking and also spalling of the outer scale. A healing subscale of $Cr_2O_3$ can be seen on the sample after spallation, but such a subscale was not protective as large amounts of sulfides could be seen both above and underneath it. The corrosion of alloy 800H in this atmosphere, therefore, is catastrophic.

The CrS stringers in the alloy substrate could have formed either by the dissociation of $Ni_3S_2$ or FeS, giving $P_{S_2}$ high enough for CrS formation, or by the $SO_2$ molecular transport through the porous sulfide phases, forming oxides which, in turn, increased the $P_{S_2}$.[3] The maximum depth of such intrusions is about 15 $\mu$m into the substrate.

Alloy 800H contains 0.4 wt.% Ti for $\gamma$-phase hardening. It is usually believed that the addition of Ti at 2–3 wt% level reduces the degradation rate, and different mechanisms have been proposed.[14–15] Taniguchi *et al.*[16] studied the effect of 0.21 wt.% Ti addition on the corrosion behavior of an Fe–23Cr–5Al alloy and concluded that Ti prevented scale spallation. It was not possible to study the effect of 0.4 wt.% Ti in this study, but it seems that some Ti was incorporated into the $Cr_2O_3$ layer.

A schematic description of the possible corrosion process before spalling is presented in Fig. 5.

## In CGA

### *Corrosion Mechanisms*

Figure 6 is the kinetics curve of alloy 800H in the $H_2-H_2S-CO-CO_2-N_2$ atmosphere. At approximately 35 hr, the sample starts to exhibit breakaway corrosion, and the corrosion rate increases with time (Fig. 6). Large nodules can be observed on the sample after 98 hr, especially around the suspension hole (Fig. 7). These have obviously been a melt during the test. XRD analysis confirmed CrS, $Cr_2O_3$, FeS, and $Fe_3O_4$ as corrosion products on the sample surface.

At locations without nodules, the preferential growth of (Cr, Fe, Mn) sulfides above the $Cr_2O_3$ scale along alloy grain boundaries are obvious (Fig. 8). Smaller sulfide particles are also found within the alloy grain regions; analysis at a higher magnification revealed that these are mainly

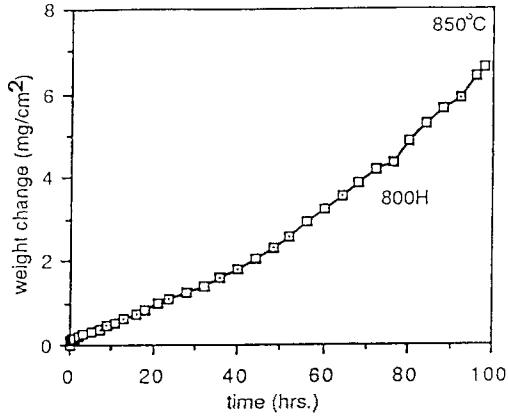


**Fig. 6.** Kinetics curve of alloy 800H in the CGA gas mixture.

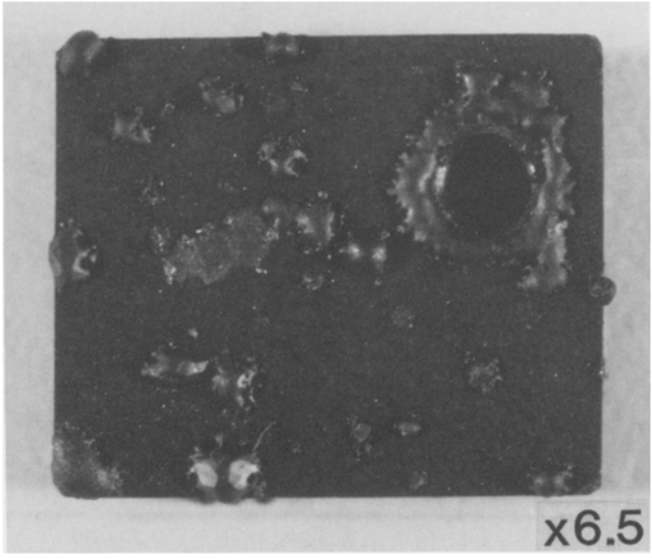


**Fig. 7.** Alloy 800H after 98 hr of corrosion at 850°C in CGA.

MnS and FeS particles as a result of outward diffusion of Mn and Fe. ZAF analysis of the corrosion-attacked grain boundaries below the $Cr_2O_3$ layer (Fig. 8) showed an enrichment of 2.1 wt.% Si, which is well above the average 1.0 wt.% Si in the alloy. Note that the data given in Fig. 8 are only relative values, as elements such as oxygen were not analyzed.

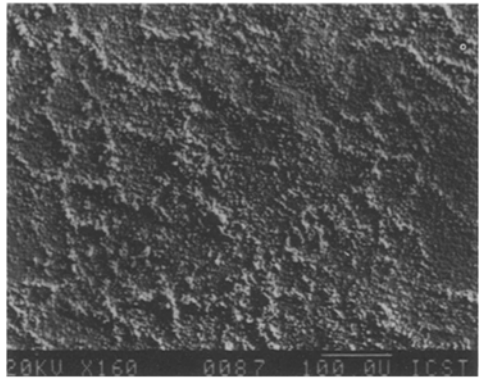

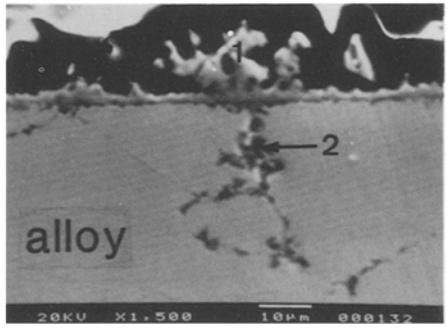


semi-quantitative EPMA (atom%)

| position | Fe | Ni | Cr | S | Mn | Si | Ti |
|---|---|---|---|---|---|---|---|
| 1 | 2.3 | 0.6 | 47.5 | 43.4 | 5.9 | 0.1 | 1.2 |
| 2 | 34.2 | 25.2 | 26.0 | 5.3 | 1.8 | 5.2 | 2.2 |

**Fig. 8.** SEM and EPMA analysis on alloy 800H after 98 hr of corrosion in CGA at 850°C.

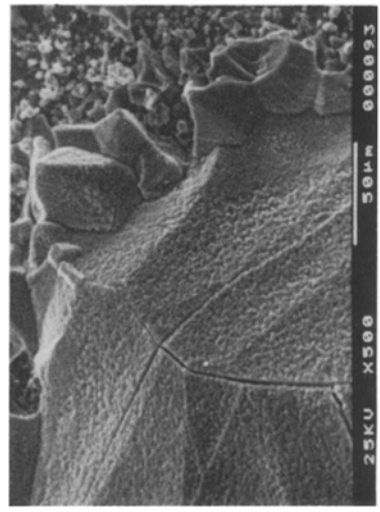
25KV X500 50µm 000093

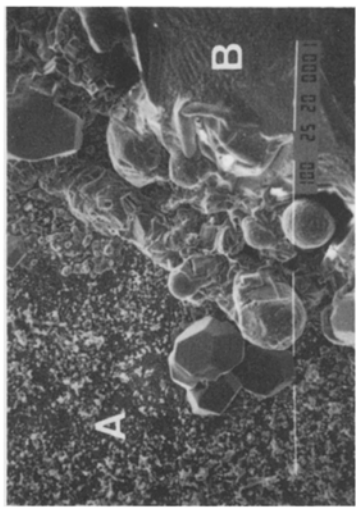
A
B


25KV X150 100µm 000092

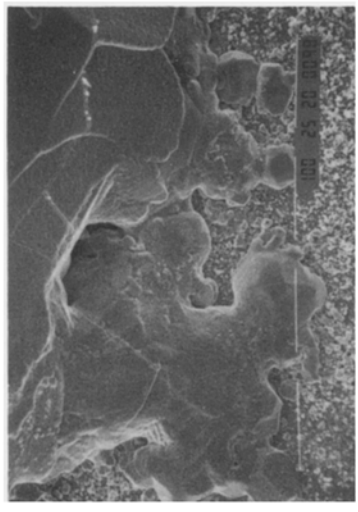

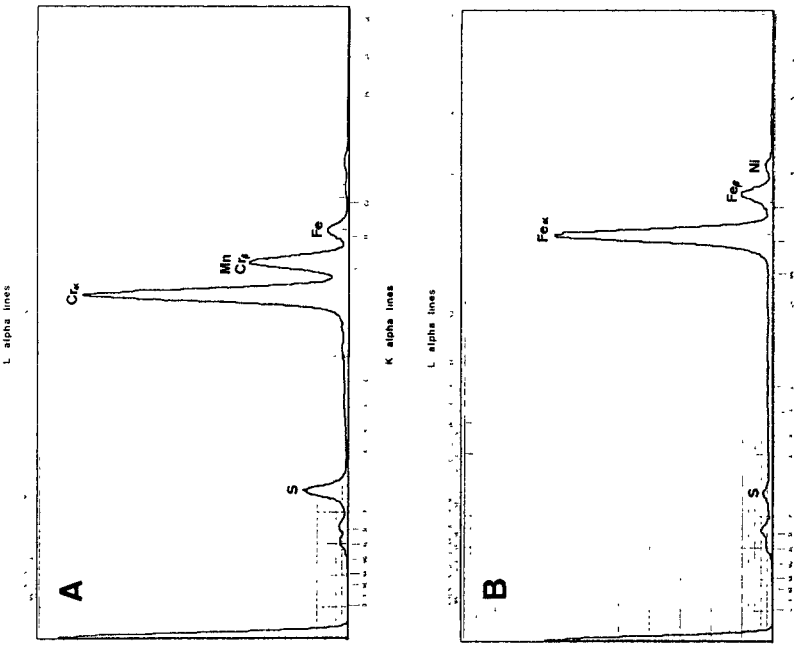


**Fig. 9.** SEM micrographs of nodules formed on alloy 800H after 98 hr of corrosion in CGA at 850°C. Four views of the sample on different locations, with EDS spectra for two areas, A and B, in the fourth picture.

A more detailed analysis of the nodules is given in Fig. 9. Most of these are faceted, but those that are not have the same features and elemental distributions. EDS analysis of the top of a nodule shows a high concentration of Fe. A cross-sectional view of one nodule is shown in Fig. 10. A crater with a lot of cavities and pores can be seen under the nodule, apparently formed as a result of the outward transport of cations. Sulfur diffused through the nodule forming (Cr, Fe, Mn) sulfide there. Below the crater, the preferential attack on grain and twin boundaries has taken place. EPMA analysis of the grain boundaries showed that, besides Fe, Ni, and Cr, there is also an enrichment of Si. The enrichment of Si on the corroded grain boundaries has also been reported by others.[17-18] The nodule itself consists of three layers, which can be seen vaguely in the SEM picture in Fig. 10 but much clearer under an optical microscope (Fig. 11). The very top thin layer is rich in Fe with no S, Ni, or Cr, and therefore must be $Fe_3O_4$ as given by XRD analysis; this is estimated to have formed from FeS upon slowly removing the sample from the hot zone after the test. An intermediate layer is rich in S, Fe, and especially Ni, but contains very little Cr. It seems that all the Ni diffused out from the crater gathered here and diffusion was still occurring just before the experiment was stopped. The major part of the nodule, however, is the innermost and largest (Cr, Fe, Mn) sulfide.

It is also interesting to note that a Ni channel, very likely in the form of $NiS_y(l)$, seems to exist in the innermost (Cr, Fe, Mn)S nodule. Such a channel was also apparent on an Ni–30Cr alloy after corrosion in a $H_2S$–$H_2$–$H_2O$ atmosphere at 900°C, although this was not mentioned by Giggin and Pettit[19] (see their Fig 23(C)). Therefore, apart from solution diffusion through the (Cr, Fe) sulfide nodule, Ni must have also migrated outward at a much faster speed as a $NiS_y(l)$ melt, through the channel.

From the thermodynamic-stability diagrams (Fig. 12), the thermodynamically stable phases in this environment are $Cr_2O_3$, FeS, Co metal, and, most important of all, $NiS_y(l)$ liquid phase. Since $P_{S_2}$ of the atmosphere is much higher than the CrS dissociation pressure, the initial stage of the corrosion is the simultaneous nucleation of $Cr_2O_3$ and CrS (see Fig. 14). The processes after this depend on the relative values of $P_{O_2}$ and $P_{S_2}$, and this is further discussed in the next section of comments on the kinetics boundary.

A schematic diagram is presented in Fig. 13 to help understand the corrosion mechanism during the breakaway. Sulfur manages to permeate through cracks or microchannels in the sulfide phase, probably in the form of $H_2S$, forming internal (Cr, Fe, Mn)S and $NiS_y(l)$. Because sulfides have a much larger volume than the metals, the ingress of sulfur causes too much pressure underneath. As a result, the $NiS_y(l)$ melt is extruded,

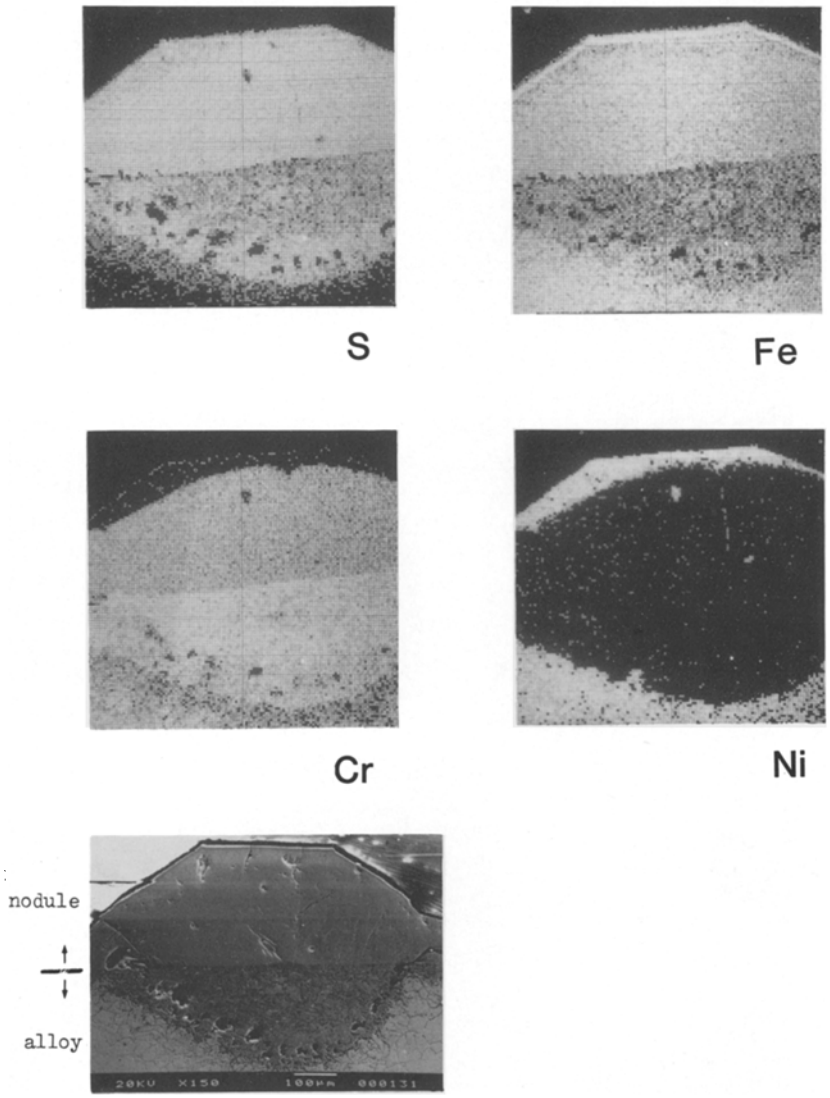


**Fig. 10.** SEM and X-ray maps of alloy 800H after 98 hr in CGA at 850°C.

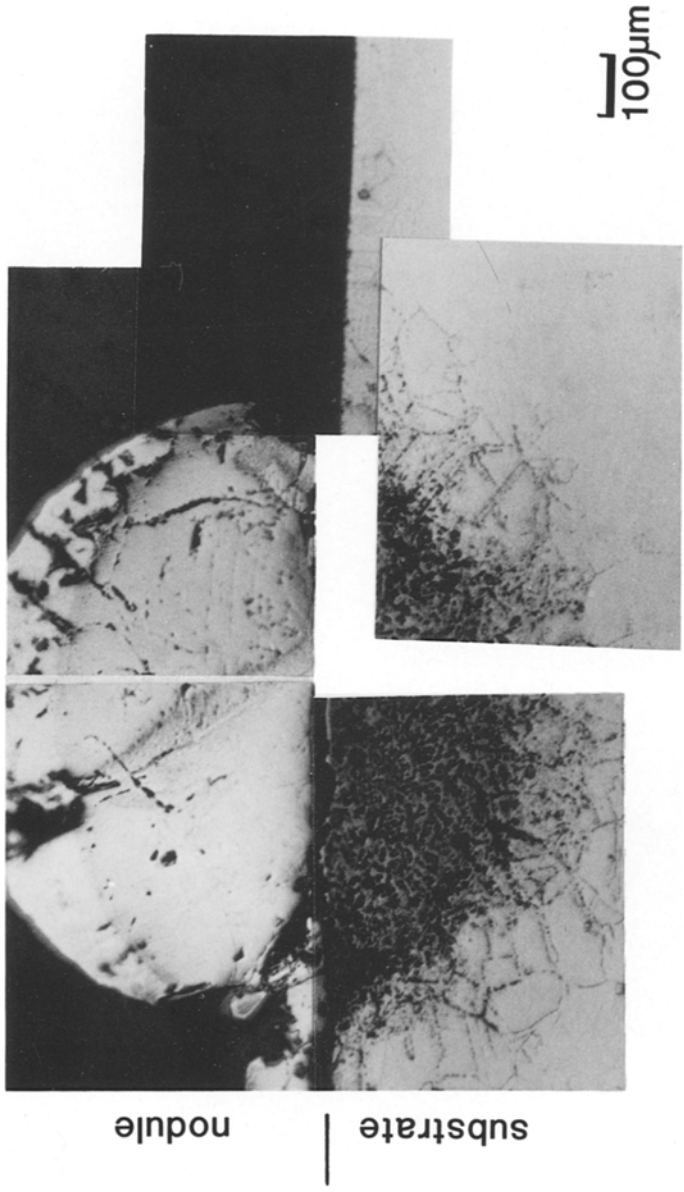


**Fig. 11.** Optical micrographs of alloy 800*H* (cross section) after corrosion in CGA for 98 hr at 850°C.

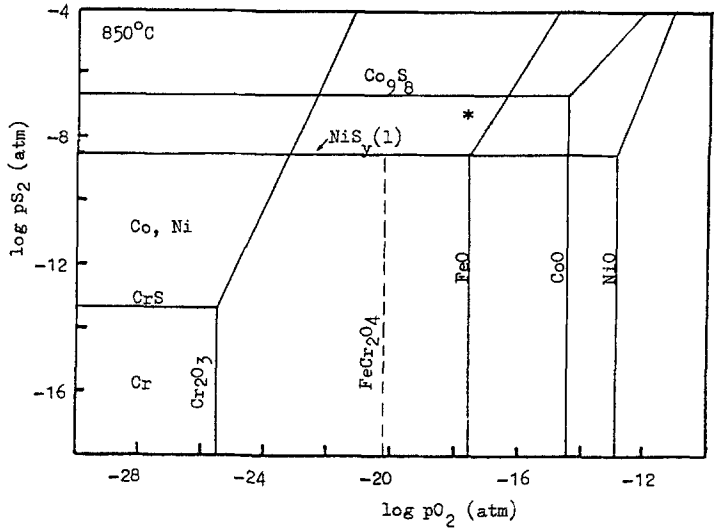


**Fig. 12.** Thermodynamic-stability diagrams for the pure metals Fe, Co, Ni, and Cr at 850°C.

through the sulfide nodule, forming a $NiS_y(l)$ cap on the (Cr, Fe, Mn) sulfide.

The very high diffusion rate of Fe allows it to diffuse through the (Fe, Cr, Mn)S nodule and the $NiS_y(l)$ phase. There is a possibility that a Ni–Fe–S melt replaces the $NiS_y(l)$ on top of the (Fe, Cr, Mn)S, as indicated in the Ni–Fe–S phase diagram.[20] On the very top of the nodule, a thin layer of the thermodynamically stable FeS is formed.

A ZAF analysis on the grain boundary below the (Cr, Fe, Mn)S pool is as follows (wt.%): 30.9 Ni, 25.1 Fe, 18.5 Cr, 3.1 S, 1.6 Si, and 0.8 Ti. The small amount of S present could mean the presence of carbides. The corrosion combination of sulfidation–carburization has already been discussed by Williams, Moller, and Grabke.[21] Indeed, carbides at such locations have been reported by Stroosnijder *et al.*,[22] also on alloy 800H.

The nodular corrosion products with sulfide pools underneath are common for Fe-base alloys corroded in CGA and have ben reported by a number of authors.[23–26]

After 95 hr of preoxidation, Baxter and Natesan[26] carried out 21 hr of CGA corrosion on Fe–25Cr–20Ni–1Zr. An FeS nodule with a sulfide pool underneath was observed. No formation of $NiS_y(l)$ on top of FeS was reported, although $NiS_y(l)$ was stable in the environment (they did find that with increasing $P_{S_2}$, the proportion of Ni in the FeS increased). This

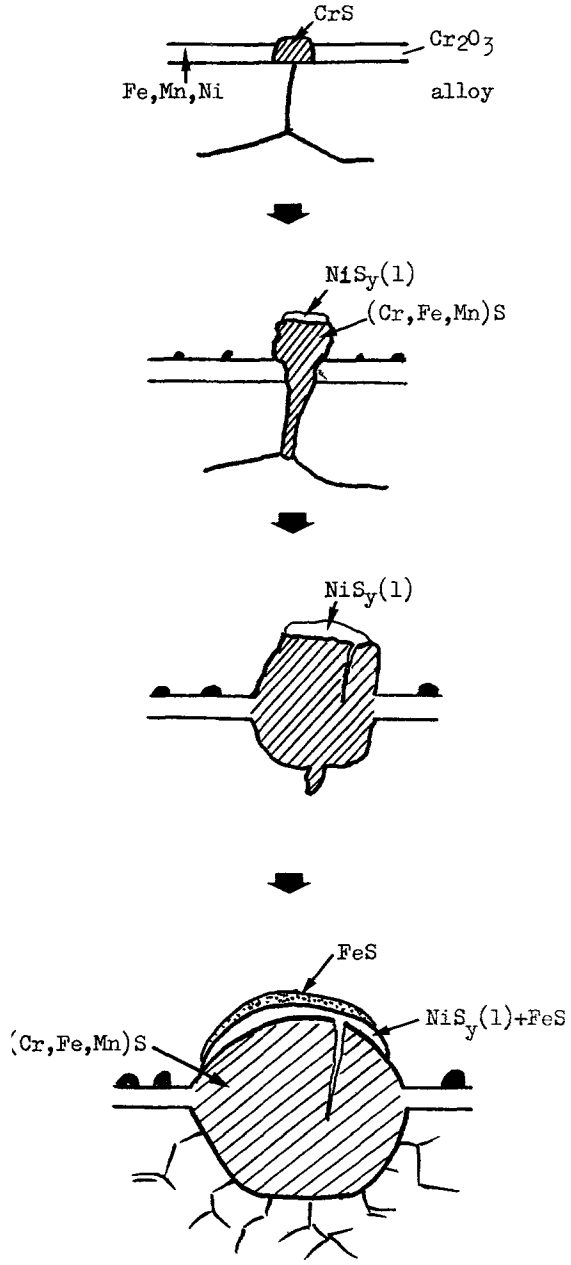


**Fig. 13.** Schematic diagrams showing the corrosion mechanism of alloy 800H in CGA at 850°C.

is probably because they did not make any detailed analysis on the nodule. Perhaps an X-ray map of the cross section of the nodule would have revealed the presence of $NiS_y(l)$.

The fact that a preoxidized alloy sample also suffers sulfidation and even breakaway corrosion brought into doubt the validity of the simultaneous sulfide–oxide nucleation mechanism. As a matter of fact, such a doubt is unnecessary and the center point is how to explain the sulfidation attack on a preoxidized sample.

A preformed $Cr_2O_3$ layer cannot prevent the outward diffusion of fast-diffusing species such as Fe, Co, Ni, Mn and the subsequent formation of their sulfides on $Cr_2O_3$. These sulfides and other possible physical defects can act as preferential locations for the inward transport of sulfur-containing species. Eventually sulfide ducts can be built up across the $Cr_2O_3$, and this is why preoxidized samples can be protective for a longer period than those without preformed $Cr_2O_3$ but still fail in the end. Indeed, Baxter and Natesan[26] reported that the point at which rapid sulfidation initiated on a preoxidized sample was marked by the formation of a continuous sulfide channel across the oxide scale.

Preoxidation treatment of an alloy, therefore, provides only very limited, and from a technical point of view, not practical, protection to the alloy. The failure of a preoxidized sample does not contradict the simultaneous-nucleation mechanism.

### *Comments on the Kinetics Boundary*

The kinetics boundary (K.B.) is defined as the $P_{O_2}$ needed for a continuous $Cr_2O_3$ layer to develop on the surface of an alloy. This is usually at least $10^2-10^3$ times higher than the $Cr_2O_3-CrS$ equilibrium value. However, this does not seem to be a strictly defined term, as it has been reported that K.B. is not an absolute value but is dependent on the exposure times.[27,28]

A schematic general model is presented in Fig. 14 for corrosion of an alloy at each side of its K.B. When on the left of the K.B., the fast-growing sulfides overgrow the $Cr_2O_3$ scale after the initial stage of simultaneous oxide and sulfide formation. Eventually, the alloy is covered by a thick layer of sulfides. No protection is available under such conditions, and severe corrosion attack is expected. Whe $P_{O_2}$ is sufficiently high or $P_{S_2}$ sufficiently low, the equilibrium point will be on the right side of the K.B. Under such conditions, the growth of the stable $Cr_2O_3$ suppresses that of the sulfides, and a continuous $Cr_2O_3$ layer is built up. However, the diffusion of fast-moving cations cannot be stopped. Fe, Ni, Co, Mn ions diffuse outward through both the $Cr_2O_3$ and the sulfide phase. Since diffusion in the sulfides is faster, sulfide ducts will be set up and sulfide

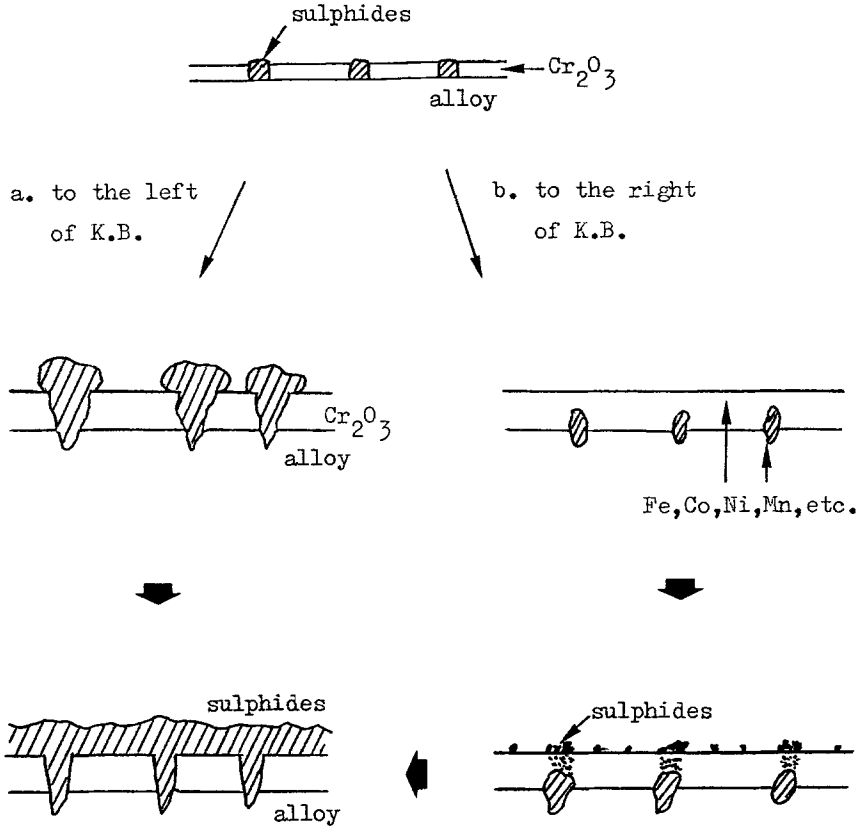


**Fig. 14.** A schematic model for the corrosion of an alloy on each side of the kinetics boundary (K.B.).

granules of those elements whose formation conditions are fulfilled will be found above the $Cr_2O_3$ scale, mostly above the sulfide ducts. On the whole, the protectivity of the oxide scale is maintained during this time but not beyond. Given enough time, sulfide channels will be set up across the oxide, and breakaway corosion will eventually take place. Therefore the value of the K.B. is only relatively valid, and most alloys will suffer breakaway in due course. The time needed is approximately the time that the sulfide channels take to develop. It might be more appropriate to define the K.B. as the $P_{S_2}$ and $P_{O_2}$ values at which an alloy is protected by a protective oxide scale for a given time period.

## ACKNOWLEDGMENTS

The authors wish to acknowledge the support from the British Council and Haynes International Ltd. for this project.

## REFERENCES

1. C. B. Alcock, M. G. Hocking, and S. Zador, *Corr. Sci.* **9**, 111 (1969).
2. K. P. Lillerud, B. Haflan, and P. Kofstad, *Oxid. Met.* **21**, 119 (1984).
3. H. Xu, M. G. Hocking, and P. S. Sidky, *Oxid. Met.* **39**, 371 (1993).
4. K. L. Luthra and W. L. Worrell, *Met. Trans. A*, **10**, 621 (1979).
5. M. LaBranche, A. Garratt-Reed, and G. J. Yurek, *J. Electrochem. Soc.* **130**, 2405 (1983).
6. R. E. Lobnig and H. J. Grabke, *Corr. Sci.* **30**, 1045 (1990).
7. K. Natesan, *Corrosion* **41**, 646 (1985).
8. D. J. Baxter and K. Natesan, *Corr. Sci.* **26**, 153 (1986).
9. V. Vasantasree and M. G. Hocking, *Corr. Sci.* **16**, 261 (1976).
10. J. K. R. Weber, Ph.D. thesis, Imperial College, London (1986).
11. P. L. Hemmings and R. A. Perkins, EPRI FP-539, Interim report (1977).
12. C. J. Smithells (Ed.), *Metals Reference Book*, 5th ed. (Butterworth, London, 1976).
13. R. P. Salisbury and N. Birks, *J. Iron Steel Inst.* **209**, 534 (1971).
14. D. R. Holmes and J. Stirnger, in *Materals to Supply the Energy Demand*, E. B. Hawbolt and A. Mitchell, eds. (ASM, 1981), p. 165.
15. T. C. Tiearney, Jr. and K. Natesan, *Oxid. Met.* **17**, 1 (1982).
16. S. Taniguchi *et al.*, *Oxid. Met.* **34**, 277 (1990).
17. O. K. Chopra and K. Natesan, *High Temp. Sci.* **9**, 243 (1977).
18. M. F. Stroosnijder and W. J. Quadakkers, *High Temp. Tech.* **4**, 141 (1986).
19. C. S. Giggins and F. S. Pettit, *Oxid. Met.* **14**, 363 (1980).
20. K. Hsieh, Y. A. Chang, and T. Zhong, *Bull. Alloy Phase Diagrams* **3**, 165 (1982).
21. D. S. Williams, R. Moller, and H. J. Grabke, *Oxid. Met.* **16**, 253 (1981).
22. M. F. Stroosnijder *et al.*, *Oxid. Met.* **33**, 371 (1990).
23. A. Rahmel *et al.*, *Oxid. Met.* **27**, 199 (1987).
24. W. F. Chu and A. Rahmel, *Oxid. Met.* **15**, 331 (1981).
25. V. Srinivasan, A. W. McCormick, and A. K. Rai, *Oxid. Met.* **34**, 401 (1990).
26. D. J. Baxter and K. Natesan, *Oxid. Met.* **31**, 305 (1989).
27. P. Kofstad, *High Temperature Corrosion* (Elsevier, New York, 1988).
28. G. Y. Yurek and K. Przybylski, *Mater. Sci. Eng.* **87**, 125 (1987).